IEEE Access
Multidisciplinary | Rapid Review | Open Access Journal

Received August 15, 2020, accepted August 27, 2020, date of publication August 31, 2020, date of current version September 14, 2020.

Digital Object Identifier 10.1109/ACCESS.2020.3020624

Robust Active Sonar Detection in Frequency and Time Dispersive Channels Using Matching Envelope Spectrum of Multi-Pulse LFM Signals

SHUAI YAO, WENHUI YU, SHILIANG FANG, AND SHUXIA HUANG
Key Laboratory of Underwater Acoustic Signal Processing, Ministry of Education, Southeast University, Nanjing 210096, China

Corresponding author: Shuai Yao (101012104@seu.edu.cn)

This work was supported in part by the National Natural Science Foundation of China under Grant 11704069, Grant 61701109, Grant 11674057, Grant 11874109, and Grant 11604048; in part by the Fundamental Research Funds for the Central Universities under Grant 2242019K30021; and in part by the Science and Technology on Sonar Laboratory under Grant 6142109180202.

ABSTRACT For detecting the target echoes undergoing distortion in frequency and time dispersive channels, a novel robust active sonar detector is proposed. The proposed active detector firstly extracts the matching envelope (ME) of the multi-pulse linear frequency modulation (LFM) signals, and then the peaks of the matching envelope spectrum (MES) contained in the designed grid searching windows are detected. The grid searching windows are designed based on the theoretical analysis of the features of the MES. Lastly, the detector utilizes the detected peaks to make a judgement for determining whether there are target echoes existing in the received signal. In addition, the proposed detector can be applied to detect the multi-pulse single frequency target echoes. The proposed active detector shows a more stable performance in the frequency and time dispersive channels, compared to several classical methods, including the replica correlation (RC), the segmented RC (SRC), and the RC integration (RCI) detectors. Simulation results validate the improved performance of the active detector, showing a gain of 0.5-4 dB compared with more standard state-of-the-art detectors. Experimental results based on sea trial data have also verified the validity and feasibility of the proposed active detector.

INDEX TERMS Active sonar detection, fast-fading distortion (FFD), matched filter, matching envelope spectrum (MES), time-spreading distortion (TSD).

I. INTRODUCTION

In active sonar systems, the matched filter has been widely used to detect the targets and estimate the target parameters [1], [2]. The active detector is designed to determine the existence of the target echoes in the received signal [3], [4]. For the linear frequency modulation (LFM) echoes reflected from the target with time-shift and plus white noise, a maximal signal-to-noise ratio (*SNR*) gain can be obtained by the coherent matched filter [5], [7]. However, for a distorted target echo, which undergoes two-way propagation and reflection by the target in shallow water, the conventional matched filter cannot achieve the promised full processing gain. Consequently, more robust active sonar detectors are needed [8]–[10].

There are two main distortion mechanisms in the underwater environment. One is modeled as fast-fading distortion (FFD), which is caused by multiple propagation paths [11]. The other one is modeled as time-spreading distortion (TSD), which is caused by the dynamics of the ocean environment [11]. To improve the performance of the active detection of the distorted target echoes, advanced model-based active detectors have been proposed. In [11], Paul M. Baggenstoss had proposed two detectors to improve the robustness of the active detectors based on the FFD and the TSD mechanisms, which are the segmented replica correlator (SRC) detector and the replica correlation integration (RCI) detector respectively. It had been proved that the SRC detector

The associate editor coordinating the review of this manuscript and approving it for publication was Chengpeng Hao.

performs better in a FFD channel while the RCI detector outperforms the SRC detector in a TSD channel. In [12], Benjamin Friedlander had generalized Baggenstoss's result to other FM signals with smooth phase functions, such as hyperbolic frequency modulation (HFM) signals. In [13], a sequential detector based on Page Test, called SST-Page test, had been proposed for the detection of active sonar target echoes in shallow-water environments. It was proved that the SST-Page test performs better than the conventional matched filter detector for the received target echoes, which are minimally spread in time.

All the detectors described in the previous section are model-based. However, due to lacking accurate knowledge of the marine environment and prior information about the target, the performance of the model-based detectors would decrease. The processing of the Page Test needs normalized density function of the matched filter output, however it cannot be obtained accurately in shallow water. Therefore, the performance of detectors based on Page Test will also decrease. Although the SRC and RCI detector are respectively the optimal detector in FFD and TSD channel, the detection performance will deteriorate when the parameters of the detectors mismatch with the dispersive level of the channel models [14]. Therefore, feature-based detection methods, which are not sensitive to inaccurate propagation models have been applied to improve the performance of the active detection [15].

In [16], a classify-before-detector, which uses so-called ''full spectrum'' feature of the received signal for adaptive detection and discrimination had been proposed. The classify-before-detector breaks through the traditional framework of detection before classification and recognition. In [17], a feature-based matched filter, which uses the feature difference of self-similarity and kurtosis of wavelet transform between the LFM signal and the noise had been proposed. Processing of the sea trial data had validated its superior performance. In [18], a method using adaptive time-frequency features for active sonar detection had been proposed. The extracted time-frequency features from the target echoes are adaptively utilized to weight the copy signal for the matched filter, and the mismatch between the transmitted signal and the target echoes can be compensated by the detector.

The performance of the conventional matched filter is also influenced by the unknown relative motion between the transmitted source and the target [19]. With no information about the target speed, many reference signals are needed to correlate with the received signal, which results in an increased computational burden [20]. To solve this problem, Dong Hun Lee *et al.* had proposed a fast target detection method by aligning a large amount of reference signals with time-shifts, and summing the time-shifted signals to construct the combined reference signal [21]. It had been proved that the proposed method is robust to the variation of unknown target speed. To solve weak target detection problem for the moving active sonar, an adaptive constant false-alarm rate (CFAR) detector, which combined underwater space-time adaptive processing model with dynamic programming based track-before-detect strategy had been proposed in [22]. Simulation results had demonstrated its better detection performance compared to the traditional anti-reverberation algorithm. For active detection of targets in a high-clutter environment, an efficient CFAR normalizer had been proposed in [23]. Statistical comparisons and specific examples had proved its high performance in regions of strong clutter. In [24], a numerical characteristic-function-based approach had been used to evaluate the CFAR detection performance. A main advantage of the numerical approach is that it is applicable to complicated background estimators.

In general, the essence of the feature-based detection method is to use the differences in characteristics between the signals and noise for detecting and discriminating the target echoes [18]. Such methods can improve the detection performance and anti-interference ability. However, these methods are still affected by the distorted channel. Therefore, the feature-based detection methods, which are robust to the channel distortion should be considered.

In this paper, we propose a novel feature-based detector to improve the robustness of the active detector against the channel distortion. For the multi-pulse echoes reflected by the target, the matching envelope (ME) is periodic while the noise is nonperiodic. Therefore, there exists different characteristics of the matching envelope spectrum (MES) between the target multi-pulse echoes and the noise or interference, and the MES of the multi-pulse LFM signals is used to detect the target echoes by the proposed detector. For the multi-pulse LFM signals, the ME is firstly extracted by using the conventional matched filter and the Hilbert transform. Then the theoretical features are analyzed for the MES of the multi-pulse LFM signals. Based on theoretical analysis of the MES features, grid searching windows matching with the MES are designed to extract the MES features. Finally, a judgement based on the extracted features of the MES is made to determine whether there are target echoes presented in the received time series. The proposed method is proved to be capable of detecting the target signals with a high robustness in frequency and time dispersive channels. Both simulation results and experimental results based on sea trial data are presented to verify the validity and feasibility of the proposed method.

The remainder of this paper is organized as follows. In Section II, the multi-pulse echo signal models received by the active sonar are firstly described respectively in an ideal channel, a time dispersive channel, a frequency dispersive channel and a channel with Doppler shift. Then the processing of the conventional and the improved matched filter are presented. Section III describes the detailed designs and implementations of the proposed detector using the MES of the multi-pulse LFM signals. And in Section IV, simulations and experimental results based on sea trial data are carried out to analyze the performance of the proposed detector. Finally, several conclusions are made in Section V.

II. PROBLEM DESCRIPTION

In this section, the echo signal models in different channels and the active detectors using the conventional and improved matched filters are respectively presented.

A. RECEIVED ECHO FROM THE TARGET

1) IN AN IDEAL CHANNEL

The complex form of the transmitted signal for the active sonar is defined as

$$s_1(t) = A\exp\left\{2\pi\left[f_1 t + \frac{\mu}{2}t^2\right] + \varphi_0\right\}\mathrm{rect}\left(\frac{t-\tau/2}{\tau}\right) \quad (1)$$

$$s(t) = \sum_{m=0}^{M-1} s_1(t - mT) \quad (2)$$

where M is the number of the transmitted pulses, A is the magnitude, τ and T are respectively the pulse duration and the pulse repetition period, f_1 is the starting frequency, μ is a constant factor defined as the frequency modulation rate, given by $(f_2 - f_1)/\tau$ and f_2 represents the end frequency, φ_0 is the initial phase, rect(t/τ) is the rectangular function with width τ. The received signals can be given by

$$r(t) = x(t) + v(t) \quad (3)$$

where $x(t)$ represents the received echo from the target and $v(t)$ represents the interference signals. The interference signal $v(t)$ is the sum of the receiver noise and the reverberation signal. For the LFM signal, it is assumed that both the receiver noise and the reverberation signal are modeled as white Gaussian random processes and independent from each other [12]. Thus, $v(t)$ can be modeled as a white zero-mean complex Gaussian random process.

In an ideal (non-distorted) channel, the received echo reflected from the target is given as

$$x(t) = \alpha e^{j\varphi} s(t - \tau_0) \quad (4)$$

where α denotes the echo attenuation, φ is a random phase uniformly distributed in $[0, 2\pi]$ and τ_0 is the two-way propagation delay. The model of the received echo from the target in an ideal channel is shown in Fig. 1.

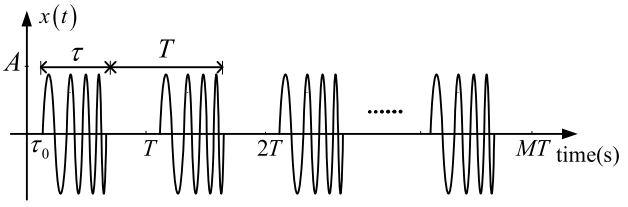

FIGURE 1. The model of the received echo from the target in an ideal channel.

2) IN DISTORTED CHANNELS

An active sonar echo undergoes distortion during two-way propagation and reflection from the target. The channel distortion can be modeled as FFD and TSD [11]. FFD is caused by dynamics of the ocean environment or uncompensated dynamics of the transmitting or receiving platforms [11]. The received waveform can be represented by the modulation of the transmitted waveform with time-varying function. Then the distorted received echo reflected from the target propagating through the FFD channel can be given by

$$x(t) = \alpha\xi(t)\, s(t) \quad (5)$$

It is assumed that $\xi(t)$ is a time-varying function and usually characterized by its bandwidth $B_c = 1/T_c$, where T_c is the coherence time.

TSD is caused by multiple propagation paths, or occurs when a transmitted waveform impinges on an extended reflector [11]. For either case, the received waveform may be represented by the convolution of the transmitted waveform with a time-spreading function. For a time-spreading function $\eta(t)$ with length T_s, the received echo reflected from the target is denoted as

$$x(t) = \int_{u=0}^{T_s} \eta(t)\, s(t - \tau_0 - u)du \quad (6)$$

It is assumed that $\eta(t)$ is a realization of a random Gaussian process that remains fixed during each experiment[11].

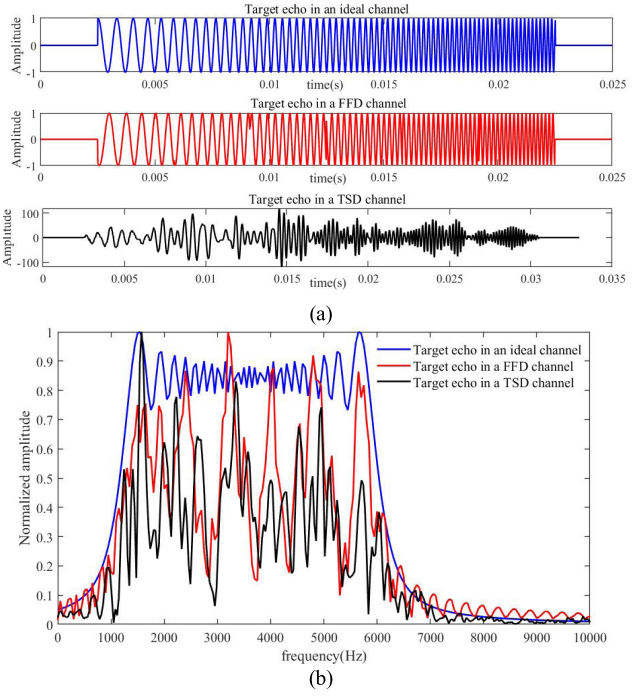

FIGURE 2. The propagated effects on the target echo in the ideal, FFD C and TSD channels. (a) The target echoes in the time domain. (b) The spectrums of the target echoes in the frequency domain.

Fig. 2 shows the propagated effects on the received echo from the target in the time and frequency domain under the ideal, FFD, and TSD channels. According to Fig. 2, it can be observed that the amplitude, frequency, or phase of the signal are modulated in the distorted channels. The pulse duration is broadened in the TSD channel and the amplitude of the spectrums in the dispersive channels fluctuate greatly.

3) IN THE CHANNEL WITH DOPPLER SHIFT

The Doppler shift is caused by the relative movement between the active sonar and the target [21]. The received echo reflected from the target with Doppler shift is given as

$$x(t) = \alpha e^{j\varphi} s((1+\delta)(t-\tau_0)) \tag{7}$$

where $\delta = 2v/c$, v is the relative movement speed between the active sonar and the target, and c is the speed of sound propagation in the sea. It is noted that v is signed, which is positive when the target moves toward to the active sonar. Conversely, it is negative when the target moves away from the active sonar. According to (7), we can see that the target echo with Doppler shift can be seen as the linear expansion or contraction of the original transmitted signal in the time domain.

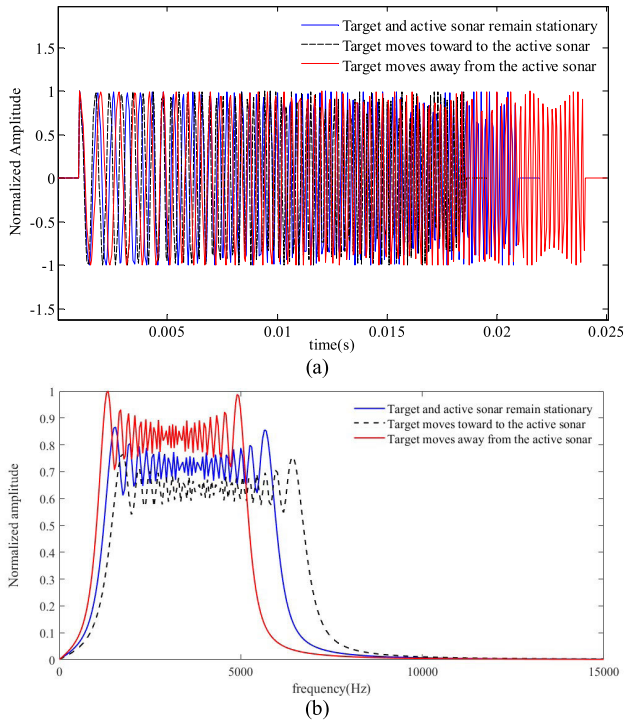

FIGURE 3. The Doppler effects on the received LFM signal in time and frequency domain. (a) The waveform of the received LFM signals with Doppler shift. (b) The spectrum of the received LFM signals with Doppler shift.

The Doppler effects on the received LFM signal in the time and frequency domain are respectively shown in Fig. 3 (a) and (b). From Fig. 3, it is worth noting that the time-domain waveforms of the LFM signal are stretched or compressed while in the frequency domain, they are shifted with a certain frequency.

B. CONVENTIONAL AND IMPROVED MATCHED FILTERS

1) MATCHED FILTERING UNDER AN IDEAL CHANNEL

The impulse and its corresponding frequency response functions of the matched filter are defined as follows:

$$h(t) = ks_1^*(t_0 - t) \tag{8}$$

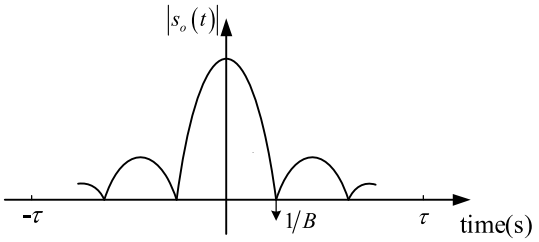

FIGURE 4. The ME of the LFM signal.

$$H(f) = kS_1^*(f)\, e^{-j2\pi f t_0} \tag{9}$$

where t_0 is the moment when the output SNR reaches the maximum value. For theoretical analysis, we assume that k is 1 and t_0 is 0, then Equation (9) can be rewritten as $h(t) = s_1^*(-t)$. Therefore, the ME of the LFM signal processed by matched filter is an approximate modulo of sinc-function [21], and it is given by (10) and shown in Fig. 4. According to (10) and Fig. 4, we can draw a conclusion that the ME has a width of $1/B$ measured from the peak to the first zero, where B is the LFM signal bandwidth. When t approaches τ, the ME will approach zero.

$$\begin{aligned} s_o(t) &= \left|\tau \sin c(\mu\tau t)\, \mathrm{rect}\left(\frac{t}{2\tau}\right)\right| \\ &= |\tau \sin c(Bt)|\, \mathrm{rect}\left(\frac{t}{2\tau}\right) \end{aligned} \tag{10}$$

In an ideal channel, the squared magnitude of the matched filter output is used by the optimal detector for active detection. Following [12], we refer to this detector as the replica correlation (RC) processor in our paper and it is given by

$$y(t) = \left|\frac{1}{\tau}\int_{u=0}^{\tau} s_1^*(\tau - u)\, r(t-u)\, du\right|^2 \tag{11}$$

The maximum of $y(t)$ is compared with a set threshold to test the presence of target echoes. The threshold (Th) under a certain false alarm probability P_f is given by $Th \geq -2\ln(P_f)$ [12].

2) IMPROVED MATCHED FILTERING UNDER DISTORTED CHANNELS

The ME defined by (10) will be distorted under time and frequency spreading channels. Therefore, the full processing gain is not achievable using the processor defined by (11), and more robust processors are needed. There are two approaches to improve the performance of the matched filter [12]. For the FFD channel, the optimal processor is the segmented replica correlator (SRC) and it is defined as

$$y(t) = \sum_{k=0}^{M_c-1}\left|\frac{M_c}{\tau}\int_0^{\tau/M_c} s_1^*\left(u + \frac{k\tau}{M_c}\right) r\left(u + t + \frac{k\tau}{M_c}\right) du\right|^2 \tag{12}$$

The pulse duration τ is divided into M_c equal segments and M_c is obtained by $M_c = \tau B$. For the case of TSD channel,

the optimal processor is the replica correlator integrator (RCI), which is defined as

$$y(t) = \sum_{k=0}^{M_s-1} \left| \frac{1}{\tau} \int_0^{\tau} s_1^* \left(u - \frac{k}{B} \right) r(t+u)\, du \right|^2 \quad (13)$$

where M_s is defined by $M_s = BT_s$ and T_s is the time-spreading length of the function $\tau(t)$. Similarly, as the RC processor, the maximum of $y(t)$ is used to judge whether there exist target echoes in the received signal, by comparing it with a detection threshold. The detection threshold of the SRC and RCI detectors under a certain false alarm probability can be approximately set by the standard chi-square distribution [11].

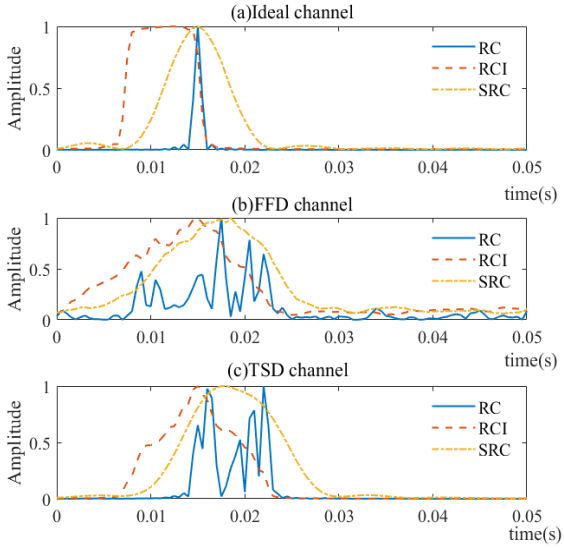

FIGURE 5. The MEs of the RC, RCI and SRC processors respectively in the ideal (a), FFD(b), and TSD(c) channels.

The processing results using the RC, SRC, and RCI processors in the ideal, FFD, and TSD channels are respectively shown in Fig. 5 (a), (b), and (c). From Fig. 5, we can see that, in an ideal channel, the RC processor performs better than the SRC and RCI processors in terms of pulse compression. In the FFD and TSD channels, the ME of the RC processor distorts seriously. Although the outputs of the SRC and RCI processors perform much better than the RC processor, the pulse compression effects of the SRC and RCI processors also suffer from serious distortion. The performance of the processors based on the ME would decrease dramatically.

III. THE PROPOSED ROBUST DETECTOR

As described in Section II, the SRC and RCI detectors can be used to improve the performance of the matched filtering in time and frequency dispersive channels. However, there still exists distortion on the ME, and the distortion results in a low robustness of the detection systems that rely on the ME for automatic detection. Therefore, in this paper, we propose a novel feature-based detector to improve the robustness of the active detector against the channel distortion. In this section, we firstly analyze the characteristics of the MES for the multi-pulse LFM signals, and then give the feature-based detector based on the extracted features of the MES. In addition, the application to the active detection of the target echo using the multi-pulse single frequency signals is also presented.

A. THE FEATURES OF THE MES

In an ideal channel, for the multi-pulse LFM signals, the ME is defined as

$$s_K(t) = \sum_{k=0}^{K-1} s_o(t - kT) \quad (14)$$

where K is the processed pulses for detection, $s_o(t)$ is the ME of the LFM signal, defined by (10). The ME of the multi-pulse LFM signals are shown in Fig. 6. From Fig. 6, it can be seen that the ME of the multi-pulse LFM signals is the modulus value of a periodic sinc-function and the repetition period is the same as that of the transmitted pulse.

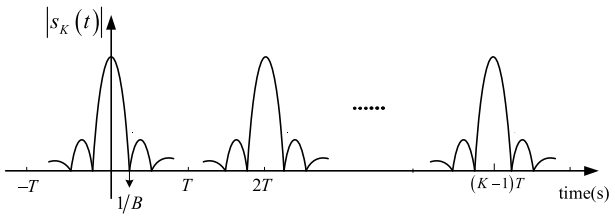

FIGURE 6. The ME of the multi-pulse LFM signals.

It is easy to get the spectrum of $s_o(t)$, that is,

$$\begin{aligned} S_0(f) &= \int_{-\infty}^{+\infty} \left| \sin c(Bt)\, \mathrm{rect}\left(\frac{t}{2\tau}\right) \right| e^{-j2\pi ft} dt \\ &= \int_{-\tau}^{+\tau} |\sin c(Bt)| e^{-j2\pi ft} dt \end{aligned} \quad (15)$$

Thus, we can derive the MES for the multi-pulse LFM signals $s_K(t)$ and it is given by

$$\begin{aligned} S_K(f) &= S_o(f) \sum_{n=0}^{K-1} e^{-j2\pi fnT} \\ &= S_o(f)\, e^{-j2\pi fT(K-1)} \frac{\sin(\pi fTK)}{\sin(\pi fT)} \end{aligned} \quad (16)$$

Substituting (15) into (16), we can get,

$$S_K(f) = \int_{-\tau}^{+\tau} |\sin c(Bt)| e^{-j2\pi ft} dt \left[\frac{\sin(\pi fTK)}{\sin(\pi fT)} \right] e^{-j\pi f(K-1)T} \quad (17)$$

The amplitude of the MES is given by

$$|S_K(f)| = \left| \int_{-\tau}^{+\tau} |\sin c(Bt)| e^{-j2\pi ft} dt \right| \left| \frac{\sin(\pi fTK)}{\sin(\pi fT)} \right| \quad (18)$$

The amplitude of the MES for the multi-pulse LFM signals is shown in Fig. 7. According to Fig. 7 and (18), we can

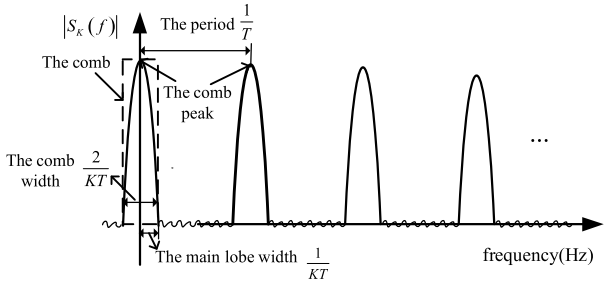

FIGURE 7. The MES of the multi-pulse LFM signals.

find that the MES is comb-shaped convergent, and has discrete comb peaks. The characteristics of the MES are mainly determined by the function of $|\sin(\pi fTK)/\sin(\pi fT)|$. We can easily draw the following key conclusions of the function of $|\sin(\pi fTK)/\sin(\pi fT)|$, and thus derive the features of the MES.

Property 1: The repetition period of $|\sin(\pi fTK)/\sin(\pi\ fT)|$ is $1/T$, which is derived as

$$\left|\frac{\sin\left[\pi\left(f+1/T\right)TK\right]}{\sin\left[\pi\left(f+1/T\right)T\right]}\right| = \left|\frac{\sin\left(\pi fTK\right)}{\sin\left(\pi fT\right)}\right| \tag{19}$$

Property 2: The main lobe width of $|\sin(\pi fTK)/\sin(\pi fT)|$ is $1/KT$, since $|\sin(\pi fTK)/\sin(\pi fT)|$ can be approximately seen as a sinc-function in the range of $[-1/2T, 1/2T]$.

Therefore, the features of the MES can be summarized as follows:

1) The frequency interval between two adjacent comb peaks is $1/T$, where T is the pulse repetition period of the multi-pulse LFM signals.

2) Each comb approximates to a sinc-function and the main lobe width (measured from the peak to the first zero) of each comb is $1/KT$ and the comb width is $2/KT$.

According to the above characteristics, it can be known that the theoretical number of the peaks existed in a certain frequency f_0 can be calculated by Tf_0 when $f \leq f_0$. In the time and frequency dispersive channels, the ME will be distorted. However, the distortion has little effect on the periodic characteristics of the MES for the multi-pulse LFM signals. In addition, the Doppler frequency shift also has little effect on the periodicity of the MES. Therefore, the characteristics of the MES in distorted channels keep well. The MEs in different channels are shown in Fig. 8 while the MESs in different channels are shown in Fig. 9.

From Fig. 8 and Fig. 9, it can be seen that the sensitivity of the MES to the channel distortion is much lower than the ME. The RC processor has the best pulse compression effect in an ideal channel. However, in other channels, the MEs of the SRC and RCI processors suffer serious time distortion or amplitude distortion. The performance of the active detection method based on comparing the maximum of the ME with set fixed threshold will deteriorate seriously. In contrast, the MESs under the various channels keep stable. As a consequence, the detectors based on the MES would be more robust than the detectors based on the ME.

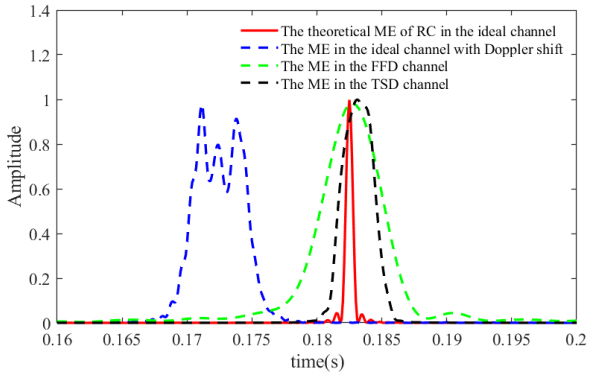

FIGURE 8. The MEs in the various channels.

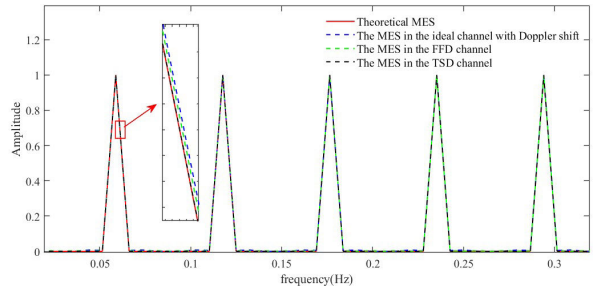

FIGURE 9. The MESs in the various channels.

B. THE DETECTION ALGORITHM BASED ON THE FEATURES OF THE MES

In this section, the active detector based on the characteristics of the MES is presented. If the target echoes exist in the received signal, the periodic discrete comb peaks will appear in the MES of the received multi-pulse signals. The peaks contained in the MES can be used to determine the presence of the target echoes. Therefore, we firstly extract the comb peaks of the MES using a designed grid searching window and then use the extracted peaks for judgement.

For the given multi-pulse LFM signals, the comb peak locations of the MES are determinative and can be theoretically calculated. Accordingly, it is only necessary to detect the presence of the peaks near the theoretical locations instead of scanning them in the entire frequency range. The flowchart of the proposed detector is shown in Table. 1.

TABLE 1. The flowchart of the proposed detector.

Algorithm: the proposed detector based on the MES
1: Matched filtering for the received signal;
2: Extract the matching envelope of the matched filter output and calculate the MES;
3: Detect the comb peaks of the MES in the designed grid searching windows;
4: Judge the presence of the target echo.

Specific implementations of step 3 and step 4 are given as follows:

(1) Design the grid searching windows.

Assuming the frequency range that we search the comb peaks is from $1/T$ (the start searching frequency) to f_0(the end searching frequency), the line spectrum frequency f_i where the comb peaks located are theoretically given by

$$f_i = \frac{i}{T} \quad i = 1, 2, \ldots, N_t \tag{20}$$

where N_t is the total number of the searching windows in the range of $1/T$ to f_0, and it is defined as

$$N_t = Tf_0 \tag{21}$$

The amplitude of the MES decreases with the increasing frequency. The searching range cannot be infinite since the comb peaks, which locate on the high frequency are hard to detect due to their small amplitudes. In this paper, we take $2T/\tau$ as the end searching frequency f_0.

The main lobe width of the ith comb can be obtained by

$$\Delta f = \frac{1}{KT} \tag{22}$$

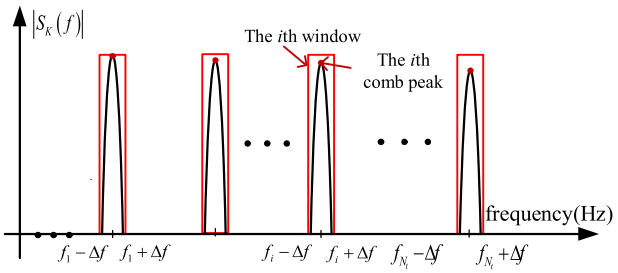

FIGURE 10. The designed grid searching windows.

Therefore, we can assume that the frequency range of the ith grid searching window is $[f_i - \Delta f, f_i + \Delta f]$ and $i = 1, 2, 3, \ldots, N_t$. The illustration of the designed grid searching windows is shown in Fig. 10. It is noted that the frequency points near the zero frequency are not considered due to the noise interference.

(2) Find the peaks in the designed grid searching windows.

According to f_i given by (20), we can find the maximum value of the MES in the ith window and record the maximum energy E_i and local signal-to-noise ratio SNR_i;

(3) Judge the presence of the peak.

If the maximum energy E_i and the local signal-to-noise ratio SNR_i are larger than the average energy and average SNR respectively in the ith searching window, we can make a judgement of that there exists a peak located on the position of the maximum f_i in the ith searching window.

(4) Count the number of peaks existing in the designed grid searching windows and denote it as N_d.

(5) Judge the presence of the target echoes by comparing N_d/N_t with the set threshold.

If N_d/N_t is lower than the set threshold, a judgement is made for that there is no target echo in the received signal, otherwise, the target echo exists in the received signal. For the set threshold, when it is set too high, the detection probability will reduce; while it is set too low, the false alarm probability will increase. In this paper, we have fixed the threshold to 0.5 following a number of experiments with difierent signals. To remedy the limitations of the fixed-threshold, we have used an adaptive threshold and made a strict judgment for the presence of the peak as shown in the step (3).

C. THE APPLICATION FOR ACTIVE DETECTION USING MULTI-PULSE SINGLE FREQUENCY SIGNALS

The proposed detector can also be applied to active detection using multi-pulse single frequency signals. The superior pulse compression effect cannot be achieved by matched filter processing for the single frequency signals. In addition, the Doppler shift has serious effects on the ME of the single frequency signals. As a consequence, instead of using the MES to detect the target echo, we directly use the envelope spectrum (ES) of the multi-pulse single frequency signals.

For the multi-pulse single frequency signals, we firstly extract the envelope of them using the proposed frequency-domain filter, then extract the features of the ES, and lastly use the detection algorithm described in section III.B to detect the target echoes.

In this paper, an improved method based on Hilbert transform is proposed to extract the envelope of the multi-pulse single frequency signals. Assuming that $\tilde{x}(t)$ is the analytic form of the real signal $x(t)$ calculated by Hilbert transform, i.e.,

$$\tilde{x}(t) = x(t) + j\hat{x}(t) \tag{23}$$

where $\hat{x}(t)$ is the Hilbert transform of $x(t)$, that is,

$$\hat{x}(t) = x(t) * \frac{1}{\pi t} \tag{24}$$

The modulus value of the analytic signal is the envelope of the real signal

$$|\tilde{x}(t)| = \left|x(t) + j\hat{x}(t)\right| = \sqrt{x^2(t) + \hat{x}^2(t)} \tag{25}$$

In the frequency domain,

$$\hat{X}(jw) = -jX(jw)\,\mathrm{sgn}(w) \tag{26}$$

where $X(jw)$ is the complex spectrum of $x(t)$ and $\hat{X}(jw)$ is the complex spectrum of $\hat{x}(t)$. According to (23) and (26), the complex spectrum $\tilde{X}(jw)$ of $\tilde{x}(t)$ can be given by

$$\tilde{X}(jw) = X(jw)(1 + \mathrm{sgn}(w)) = \begin{cases} 0 & w < 0 \\ 2X(jw) & w > 0 \end{cases} \tag{27}$$

Therefore, we can obtain the envelope of $x(t)$ by calculating the inverse Fourier transform of $\tilde{X}(jw)$. It is easy to see that the above envelope-extraction algorithm using Hilbert transform has a major problem of that noise in the whole frequency band are passed. To solve this problem, we propose a frequency-domain filtering method to suppress the noise. The definition of frequency-domain filter is given as

$$H_F(jw) = \begin{cases} 2 & w_1 < w < w_2 \\ 0 & otherwise \end{cases} \tag{28}$$

where w_1 and w_2 are the lower and upper limit of frequency-domain filter. The envelope of signal can be expressed by

$$y(t) = IFFT\{X(jw) H_F(jw)\} \tag{29}$$

where $IFFT\{\bullet\}$ denotes Inverse Fast Fourier Transform. Now, we analyze the processing gain of the proposed filter. The input *SNR* of the filter can be given by

$$SNR_{in} = A^2 \Big/ \sigma^2 \tag{30}$$

where σ^2 is the variance of the noise. We denote B_w as the bandwidth of the frequency-domain filter, and $B_w = w_2\text{-}w_1$. The output *SNR* of filter can be calculated by

$$SNR_{out} = A^2 W \Big/ B_w \sigma^2 \tag{31}$$

And the processing gain of the filter is

$$G_{opt} = \frac{SNR_{out}}{SNR_{in}} = \frac{W}{B_w} \tag{32}$$

where W is $f_s/2$. Considering the Doppler frequency shift, the B_w is set as $0.02f_1$ in our paper. The proposed frequency-domain filter for extracting the envelope provides a high output *SNR* while the computational load is greatly reduced, compared with the conventional bandpass filter in the time domain, which needs twice Fourier transforms and one complex multiplication.

For the multi-pulse single frequency signals in an ideal channel, the form of ES can be derived as follows:

$$u_K(t) = \sum_{k=0}^{K-1} u_s(t - kT) \tag{33}$$

where $u_s(t)$ is defined by $u_s(t) = A\ \mathrm{rect}((t\text{-}\tau/2)/\tau)$ and the spectrum of $u_s(t)$ is

$$U_s(f) = A\tau \sin c(f\tau) e^{-j\pi f\tau} \tag{34}$$

The ES of the multi-pulse single frequency signals is

$$U_K(f) = A\tau \sin c(f\tau) \left[\frac{\sin(\pi fTK)}{\sin(\pi fT)}\right] e^{-j\pi f[(K-1)T+\tau]} \tag{35}$$

Thus, the amplitude of the ES is given by

$$|U_K(f)| = A\tau \left|\sin c(f\tau) \frac{\sin(\pi fTK)}{\sin(\pi fT)}\right| \tag{36}$$

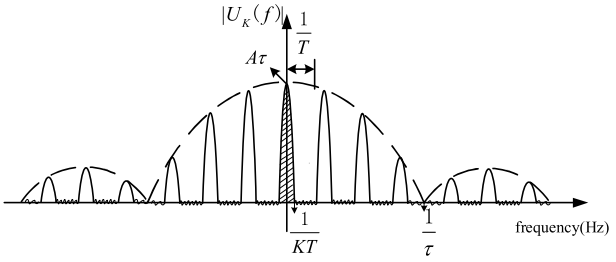

FIGURE 11. The ES of the multi-pulse single frequency signals.

The ES of the multi-pulse single frequency signals is shown in Fig. 11. According to (36) and Fig. 11, we can see that the ES of the multi-pulse single frequency signals has similar characteristics with the MES of the multi-pulse LFM signals. The analysis for the MES is still suitable for the ES of the multi-pulse single frequency signals.

IV. SIMULATIONS AND EXPERIMENTS

In this section, we evaluate the performance of the proposed detector by comparing it with the existed state-of-the-art active detectors based on matched filtering including the RC, SRC, and RCI detectors for both simulated signals and sea trial data.

A. SIMULATION RESULTS

The transmitted multi-pulse LFM signal is generated according to (1) and (2). The duration τ is set 0.256s, the period T is set 17s, the starting frequency f_1 is set 3.1 kHz and the frequency modulation rate μ is set 0.4 kHz/s. The number of transmitted pulses M is set 10 and the sample frequency f_s is set 10 kHz.

The received signal $r(t)$ is generated according to the complex form of (3). The variance σ^2 of the noise $v(t)$ is set to be 1. The *SNR* is defined in decibels (dB) as $SNR = 10\lg(A^2/\sigma^2)$. For the received echo from the target $x(t)$ in an ideal, FFD, TSD channel and with Doppler shift are respectively generated according to (4), (5), (6), and (7).

Similarly with [11], for simplifying the evaluation of the detection performance, we assume that the time-varying function $\xi(t)$ of the FFD channel is piecewise constant with segment length T_c, and $M_c = \tau/T_c$ is the number of segments. The piecewise constant is generated by a complex Gaussian random process with zero mean and unit variance. In the simulations, T_c is set 0.0427s and M_c is set 6. The received signal in the FFD channel is simulated by multiplying the signal with the piecewise constant. For each pulse of the simulated multi-pulse LFM signals in the FFD channel, we use different piecewise constant. The length T_s of the time-varying function $\eta(t)$ of the TSD channel is set 3.2ms. For each pulse of the simulated multi-pulse LFM signals in the FFD channel, we also use different random $\eta(t)$ with the same time length T_s.

For the SRC and RCI detectors, we assume that the parameters of the detectors match with the dispersive level of the channel models. In this case, the SRC and RCI detectors perform best in the FFD and TSD channel respectively. The segments M_c of the SRC detector is set 6 and the M_s of the RCI detector is 0.3277s, which is calculated by $M_s = BT_s$.

We firstly analyze the characteristics of the MES for the simulated multi-pulse LFM signals in various channels to verify the stability of the MES. The number of the processed pulses for detection K is set 6 and the *SNR* is set -5dB. The MESs in different channels for the multi-pulse LFM signals are respectively shown in Fig. 12 to Fig. 17. Fig. 12 shows the MES in an ideal channel. Fig. 13 represents the MES for a moving target with a speed of 20knots. Fig. 14 and Fig. 15 respectively show the MESs under the FFD and TSD

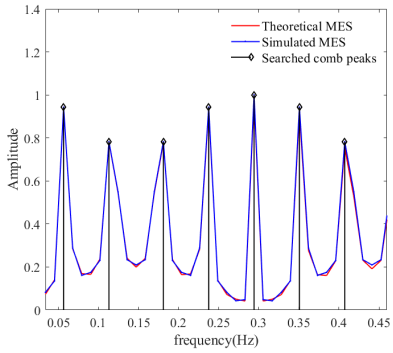

FIGURE 12. The MES under an ideal channel.

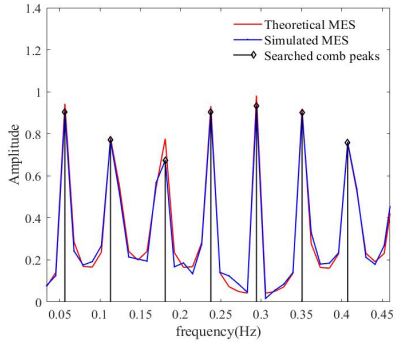

FIGURE 13. The MES under an ideal channel with Doppler shift (20 knots of target speed).

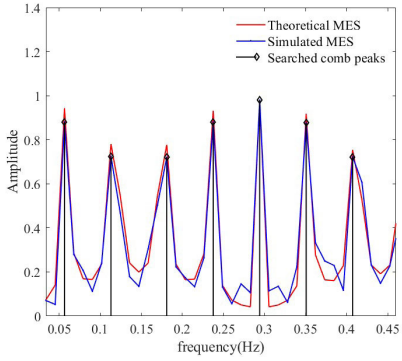

FIGURE 14. The MES under a FFD channel.

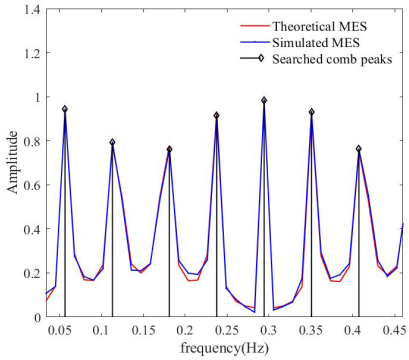

FIGURE 15. The MES under a TSD channel.

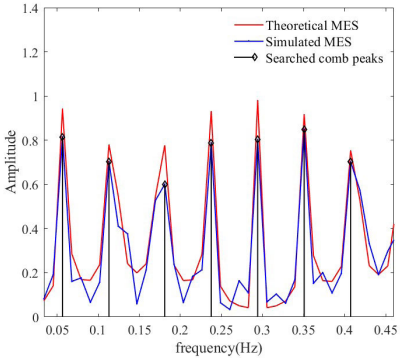

FIGURE 16. The MES under a FFD channel with Doppler shift (20 knots of target speed).

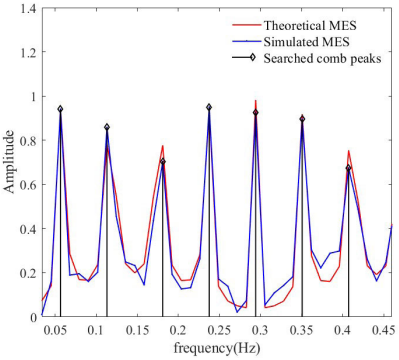

FIGURE 17. The MES under a TSD channel with Doppler shift (20 knots of target speed).

channel. Fig. 16 and Fig. 17 show the MESs under the FFD and TSD channel with Doppler shift.

From Fig. 12-17, it can be seen that the comb peaks of the MESs under different channels are obvious and periodic. The periodic characteristics of the MES for the multi-pulse LFM signals under different channels are stable. Therefore, the periodic characteristics of the MES can be used to detect the target echoes robustly.

Now, we assess the performance of the active detectors by plotting the detection probability P_d versus different *SNR*s starting from -25 to 0 dB in a step of 1 dB in various channels including ideal, ideal with Doppler shift, FFD, TSD, FFD and TSD with Doppler shift channels. For each *SNR*, 1000 times Monte Carlo experiments are run. In each experiment, the threshold of the RC, SRC, and RCI detector is determined analytically for a false alarm probability of 0.1%.

Fig. 18 shows the detection probability P_d versus *SNR*s in various channels for active detection of the LFM target echoes. Fig. 18 (a) presents the detection performance for an ideal channel, (b) presents the results for an ideal channel with Doppler shift, (c) corresponds to the FFD channel, (d) depicts the results for a TSD channel, (e) corresponds to the FFD channel with Doppler shift, and (f) depicts the results for the TSD channel with Doppler shift. In each figure, the solid line corresponds to the proposed active detector.

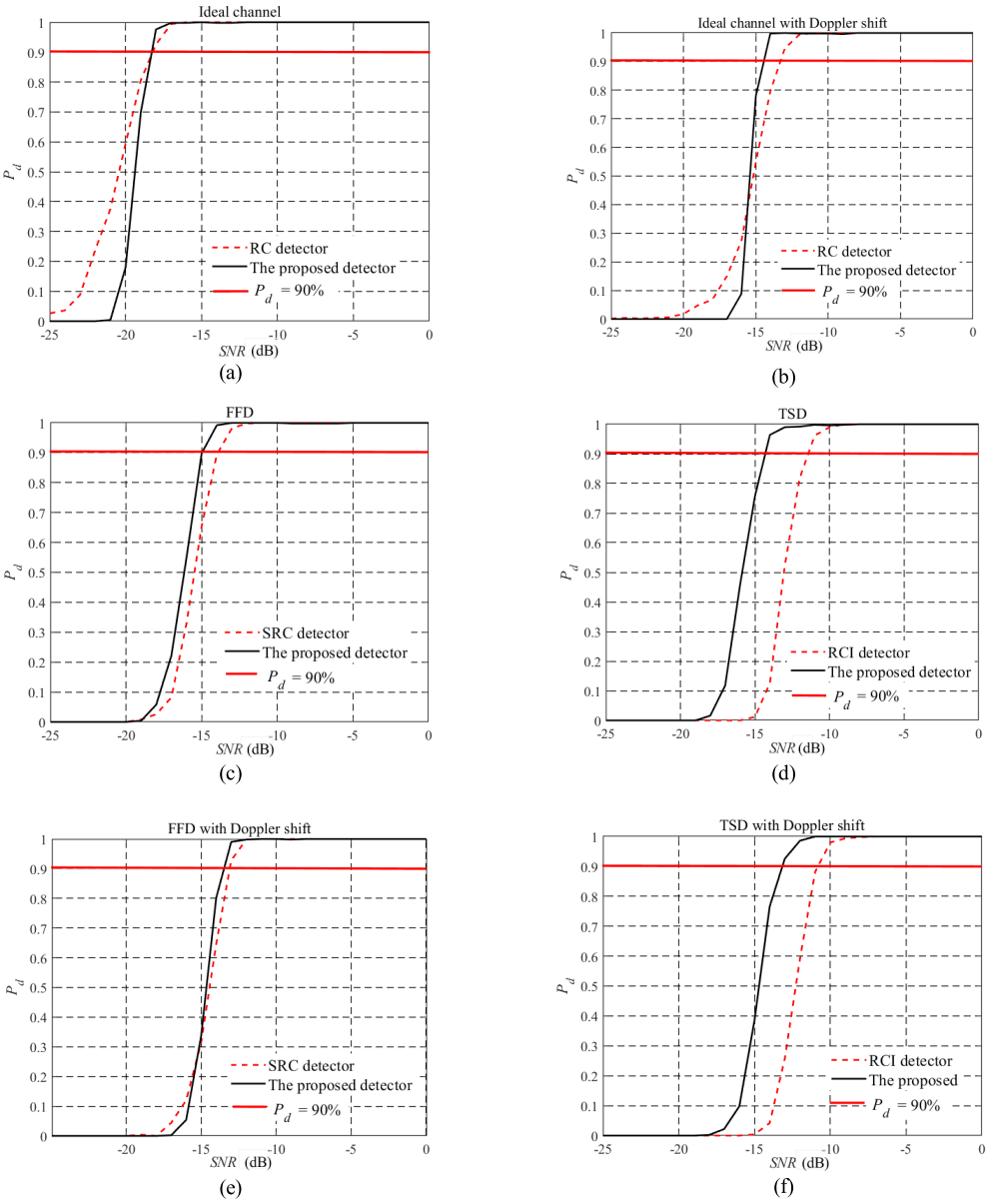

FIGURE 18. **Detection probability P_d versus *SNR*s in the various channels. (a) in an ideal channel. (b) in an ideal channel with Doppler shift. (c) in a FFD channel. (d) in a TSD channel. (e) in a FFD channel with Doppler shift. (f) in a TSD channel with Doppler shift.**

The performance is measured by the relative *SNR* required for a detection probability of 90%. According to Fig. 18 (a), we observe that, in an ideal channel, the performance of the proposed detector is worse than the RC detector when *SNR* is less than −18dB, however, when the *SNR* is larger than −18dB, the proposed detector performs better. In terms of the relative *SNR* required for detection probability of 90%, it performs similarly with the optimal RC detector.

Considering the Doppler shift as shown in Fig. 18 (b), we can see that the RC detector outperforms the proposed detector when the *SNR* is less than −16dB. It is caused by that, when the *SNR* is too low, some peaks in the designed grid searching windows are not successfully detected by the proposed detector, while the peak value of the RC processor output is not so sensitive to the small Doppler shift and high Gaussian noise. In the aspect of the relative *SNR* required for detection probability of 90%, the performance loss of the RC detector relative to the proposed detector's is 1.5dB.

While in the FFD channel as shown in Fig. 18 (c), the proposed detector shows up to 1dB gain relative to the SRC detector. The proposed detector also exhibits a better performance in the TSD channel as shown by Fig. 18 (d) and the performance gain of the proposed detector relative to the RCI detector is 4dB. Considering the Doppler shift in the FFD and TSD channel as shown by Fig. 18 (e) and (f), the proposed detector outperforms the SRC and RCI detector 0.5dB and

3.5dB respectively measured by the relative *SNR* required for detection probability of 90%.

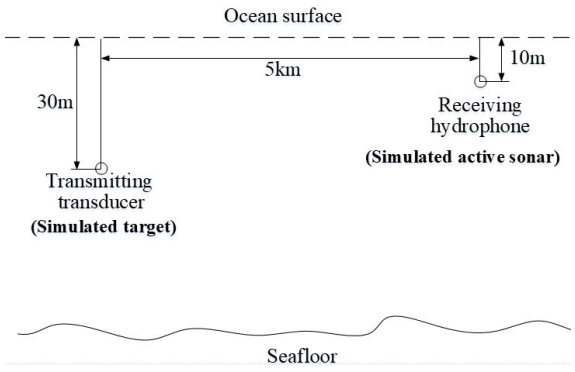

FIGURE 19. Schematic diagram of the sea trial.

B. EXPERIMENTAL RESULTS BASED ON REAL SEA TRIAL DATA

In the sea trial, we have simulated the one-way propagation from the target to the active sonar and the schematic diagram of the sea trial is shown in Fig. 19. The sea trial was carried out in the East China Sea. As shown in Fig. 19, the target was simulated using a transmitting transducer, which is 30 m to the ocean surface while the active sonar was simulated using a receiving hydrophone, which is 10 m to the ocean surface. Both the transmitting transducer and receiving hydrophone are single and omnidirectional. The distance between the transmitting transducer and the receiving hydrophone is about 5 km. In the sea trial area, the propagation speed of the sound presented a weak negative gradient velocity distribution. Two cases of the experimental results based on real sea trial data including multi-pulse LFM and single frequency signals are given to validate the feasibility of the proposed active detector.

Case 1 (Sea Trial Data Contain the Multi-Pulse LFM Signals): In this case, we analyze the real sea trial data, which contains the multi-pulse LFM signals to validate the feasibility of the proposed active detector. The parameters of the signal are same as the simulated multi-pulse LFM signal in section IV. A. The number of the transmitted pulses M is 6. We firstly analyze the MEs of the RC, SRC, and RCI detectors and then give the detection results of the sea trial data using the proposed detector.

Fig. 20 demonstrates the time domain signal, the amplitude-normalization power spectrum and time-frequency distribution (TFD). Fig. 21 shows the MEs processed by the RC, SRC, and RCI processors. According to Fig. 21, we can see that the envelopes of all the LFM signals are easy to detect, however the detection performance is sensitive to the set threshold. As shown in Fig. 21, there are six LFM pulses contained in the sea trial data. When the threshold is set as 0.5, 3 pulses can be detected for the RC processor, only 1 pulse can be detected for both the SRC and RCI processors. When the threshold is set as 0.2, 6, 3 and 4 pulses are respectively

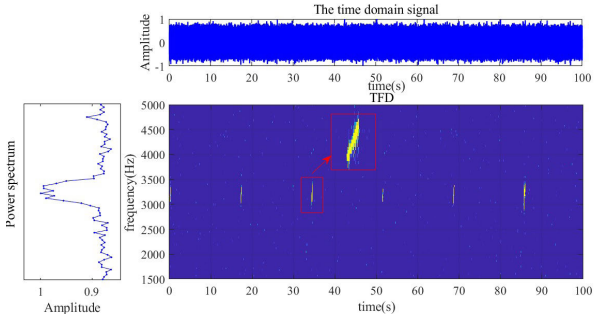

FIGURE 20. The time domain signal, amplitude-normalization power spectrum, and time-frequency distribution (TFD).

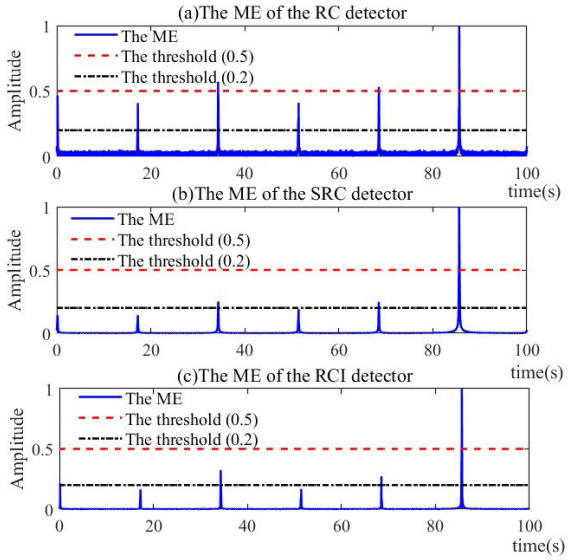

FIGURE 21. The MEs of the RC (a), SRC (b), and RCI (c) processors.

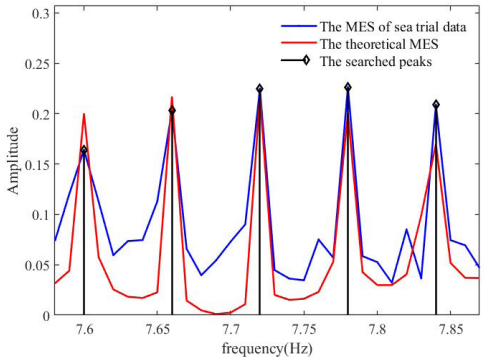

FIGURE 22. The theoretical MES, the MES of the sea trial data and the searched peaks.

detected for the RC, SRC, and RCI processors. Fig. 22 shows the theoretical MES, the MES of the sea trial data and the searched peaks of the MES for the sea trial data. It is worth noting that the MES of the sea trial data approaches the theoretical MES and the peaks can be easily detected.

The processed pulses for detection K is set from 3 to 6 in a step of 1. The number of the theoretical comb peaks N_t is calculated by (21) and the number of the extracted peaks N_d

TABLE 2. The detection results of case 1 using the proposed detector.

Number of the processed pulses K	Number of the theoretical comb peaks N_t	Number of the extracted peaks N_d	The ratio of N_d to N_t
3	129	63	48.84%
4	129	65	50.39%
5	129	69	53.4%
6	129	74	57.36%

are recorded. The detection results for the real sea trial data using the proposed detector are shown in Table.2. According to Table. 2, it can be observed that the ratioes are larger than the set threshold of 0.5 when $K > 3$ and the number of the extracted peaks N_d increases with the number of the processed pulses K, which would improve the detection performance. However, more processed pulses will burden the computation load and storage space. Therefore, in practical sonar applications, both the requirements of the computation load and real-time should be comprehensively considered to determine the number of the processed pulses K.

Case 2 (Sea Trial Data Contain the Multi-Pulse Single Frequency Signals): In this case, we consider the real sea trial data, which contains multi-pulse single frequency signals to verify the application of the proposed detector for active detection using multi-pulse single frequency signals. The duration τ of the single frequency signals transmitted from simulated target is set 0.07s, the period T is set 4.56s, the frequency f_1 is set 3.1kHz. The number of the transmitted pulses M is 9 and the sample frequency is set 10 kHz. We also firstly analyze the extracted envelopes using different methods and then give the detection results of the sea trial data using the proposed detector.

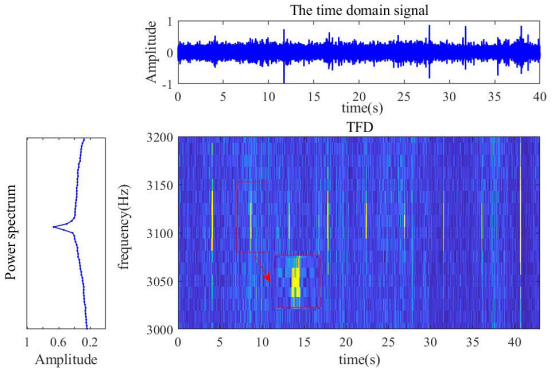

FIGURE 23. The time domain signal, amplitude-normalization power spectrum, and time–frequency distribution (TFD).

Fig. 23 demonstrates the time domain signal, amplitude-normalization power spectrum and time-frequency distribution (TFD). Fig. 24 shows the extracted envelope using the Hilbert transform and bandpass filter in time domain and the proposed frequency-domain filter.The bandwidth of the bandpass filter in time domain is set the same as the proposed frequency-domain filter. We can observe that the

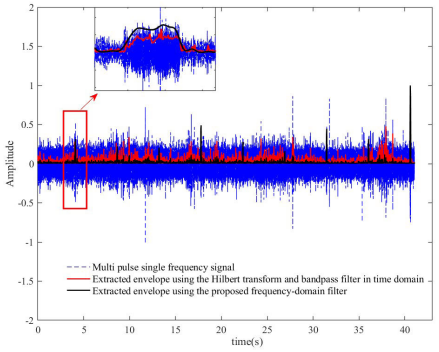

FIGURE 24. The extracted envelopes of the sea trial data using different methods.

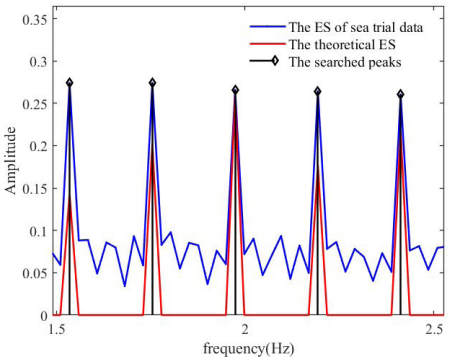

FIGURE 25. The theoretical ES, the ES of the sea trial data and the searched peaks.

amplitude fluctuation of the extracted envelope using the proposed frequency-domain filter is less than that using the Hilbert transform and bandpass filter in the time domain. Fig. 25 shows the theoretical ES, the ES of the sea trial data and the searched peaks of the ES for the sea trial data. According to Fig. 25, we can see that the peaks of the ES of the sea trial data approaches the theoretical ones and the peaks are can be extracted accurately.

The detection results of the sea trial data using the proposed detector are shown in Table. 3. According to Table. 3, a conclusion can be drawn that the ratios are larger than the threshold of 0.5 when $K > 3$.

TABLE 3. The detection results of case 2 using the proposed detector.

Number of the processed pulses K	Number of the theoretical comb peaks N_t	Number of the extracted peaks N_d	The ratio of N_d to N_t
3	114	48	41.74%
4	114	60	52.63%
5	114	68	59.65%
6	114	79	69. 30%
7	114	97	85.09%
8	114	111	97.37%
9	114	112	98.25%

V. CONCLUSION

In this paper, we propose a novel active detector based on the MES of the multi-pulse LFM signals for detecting the

target echoes undergoing distortion in frequency and time dispersive channels. The MES of the multi-pulse signals appears to be periodic comb peaks and the periodic characteristics of the MES keeps well in spite of the target echoes undergoing distortion. The proposed method makes use of the prior information of the transmitted signal to calculate the theoretical comb-peak locations of the MES. According to the theoretically calculated locations, the comb peaks of the MES are searched.

The key procedures of the proposed active detector consist of matched filtering for the received signal, extracting the envelope of the matched filter output and calculating the MES, detecting the comb peaks of the MES in the designed grid searching windows and judging the presence of the target echo. Simulation results show that the proposed method outperforms the RC, SRC, and RCI detectors with a gain of 0.5 to 4 dB in terms of the relative *SNR* required for a detection probability of 90%. In addition, experimental results based on sea trial data have proved the validity of the proposed detector.

The focus of this paper has been on presenting techniques for active detection of the target echoes whose periodicity property keeps well. However the periodicity property of the target echoes may be disturbed by strong clutter or multi-target signals. We believe that the full potential of the proposed approach is not yet exploited. To detect the target echoes, whose periodicity property is disturbed by strong clutter or multi-target signals coming from different direction of arrivals, beamforming technologies can be combined to get better results. In addition, the same methodology can also be applied to radar for detecting the target echoes whose periodicity property keeps well.

ACKNOWLEDGMENT

The authors would like to thank the anonymous reviewers for their useful comments and suggestions.

REFERENCES

[1] T. H. Glisson, C. I. Black, and A. P. Sage, "On sonar signal analysis," *IEEE Trans. Aerosp. Electron. Syst.*, vol. AES-6, no. 1, pp. 37–50, Jan. 1970.
[2] W. C. Knight, R. G. Pridham, and S. M. Kay, "Digital signal processing for sonar," *Proc. IEEE*, vol. 69, no. 11, pp. 1451–1506, Nov. 1981.
[3] Y. Sun, P. Willett, and R. Lynch, "Waveform fusion in sonar signal processing," *IEEE Trans. Aerosp. Electron. Syst.*, vol. 40, no. 2, pp. 462–477, Apr. 2004.
[4] X. Song, P. Willett, and S. Zhou, "Range bias modeling for hyperbolic-frequency-modulated waveforms in target tracking," *IEEE J. Ocean. Eng.*, vol. 37, no. 4, pp. 670–679, Oct. 2012.
[5] W. S. Burdic, *Underwater Acoustics System Analysis*. Newport Beach, CA, USA: Peninsula, 2002.
[6] D. W. Ricker, *Echo Signal Processing*. Norwell, MA, USA: Klewer, 2003.
[7] P. R. Atkins, T. Collins, and K. G. Foote, "Transmit-signal design and processing strategies for sonar target phase measurement," *IEEE J. Sel. Topics Signal Process.*, vol. 1, no. 1, pp. 91–104, Jun. 2007.
[8] J. A. Tague, C. M. Pike, and E. J. Sullivan, "Active sonar detection in multipath: A new bispectral analysis approach," *Circuits Syst. Signal Process.*, vol. 13, no. 4, pp. 455–466, Dec. 1994.
[9] N. M. Sasi, P. S. Sathidevi, R. Pradeepa, and S. Gopi, "A low complexity STAP for reverberation cancellation in active sonar detection," in *Proc. IEEE Sensor Array Multichannel Signal Process. Workshop*, Jerusalem, Israel, Oct. 2010, pp. 245–248.
[10] S. Jeong, S.-W. Ban, S. Choi, D. Lee, and M. Lee, "Surface ship-wake detection using active sonar and one-class support vector machine," *IEEE J. Ocean. Eng.*, vol. 37, no. 3, pp. 456–466, Jul. 2012.
[11] P. M. Baggenstoss, "On detecting linear frequency-modulated waveforms in frequency- and time-dispersive channels: Alternatives to segmented replica correlation," *IEEE J. Ocean. Eng.*, vol. 19, no. 4, pp. 591–598, 1994.
[12] B. Friedlander and A. Zeira, "Detection of broadband signals in frequency and time dispersive channels," *IEEE Trans. Signal Process.*, vol. 44, no. 7, pp. 1613–1622, Jul. 1996.
[13] D. A. Abraham and P. K. Willett, "Active sonar detection in shallow water using the page test," *IEEE J. Ocean. Eng.*, vol. 27, no. 1, pp. 35–46, Jan. 2002.
[14] X. M. Zhou, "A new approach for estimating the coherence time of fast fading distortion channels," *Appl. Acoust.*, vol. 29, no. 1, pp. 23–27, 2010.
[15] T. L. Hemminger and Y.-H. Pao, "Detection and classification of underwater acoustic transients using neural networks," *IEEE Trans. Neural Netw.*, vol. 5, no. 5, pp. 712–718, Sep. 1994.
[16] F. B. Shin and D. H. Kil, "Full-spectrum signal processing using a classify-before-detect paradigm," *J. Acoust. Soc. Amer.*, vol. 99, no. 4, pp. 2188–2197, Apr. 1996.
[17] J. Li and C. H. Hou, "Multi-scale feature-based matched filter processing," *Acta Acustica, English*, vol. 23, no. 4, pp. 331–339, 2004.
[18] L. Zou, K. Tan, and J. Zha, "Active sonar detection using adaptive time-frequency feature," in *Proc. IEEE/OES China Ocean Acoust. (COA)*, Harbin, China, Jan. 2016, pp. 1–4.
[19] R. Tao, N. Zhang, and Y. Wang, "Analysing and compensating the effects of range and Doppler frequency migrations in linear frequency modulation pulse compression radar," *IET Radar, Sonar Navigat.*, vol. 5, no. 1, pp. 12–22, Jan. 2011.
[20] S. Kay and J. Salisbury, "Improved active sonar detection using autoregressive prewhiteners," *J. Acoust. Soc. Amer.*, vol. 87, no. 4, pp. 1603–1611, Apr. 1990.
[21] D.-H. Lee, J.-W. Shin, D.-W. Do, S.-M. Choi, and H.-N. Kim, "Robust LFM target detection in wideband sonar systems," *IEEE Trans. Aerosp. Electron. Syst.*, vol. 53, no. 5, pp. 2399–2412, Oct. 2017.
[22] M. Wei, B. Shi, C. Hao, and S. Yan, "A novel weak target detection strategy for moving active SONAR," in *Proc. OCEANS MTS/IEEE Kobe Techno-Oceans (OTO)*, Kobe, Japan, May 2018, pp. 1–6.
[23] F. W. Bentrem, J. Botts, and J. E. Summers, "Design of a signal normalizer for high-clutter active-sonar detection," *J. Acoust. Soc. Amer.*, vol. 143, no. 3, p. 1760, 2018.
[24] D. A. Abraham, "Performance analysis of constant-false-alarm-rate detectors using characteristic functions," *IEEE J. Ocean. Eng.*, vol. 43, no. 4, pp. 1075–1085, Oct. 2018.

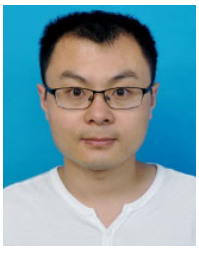

SHUAI YAO received the B.S. degree from the Ocean University of China, Qingdao, China, in 2005, and the Ph.D. degree from Southeast University, Nanjing, China, in 2016. He is currently a Lecturer with the Key Laboratory of Underwater Acoustic Signal Processing, Ministry of Education, Southeast University. His research interests include underwater acoustic signal processing, array signal processing, parameter estimation, and signal detection.

WENHUI YU was born in Zhangjiakou, China, in 1995. She is currently pursuing the B.S. degree with the Key Laboratory of Underwater Acoustic Signal Processing, Ministry of Education, Southeast University (SEU). Her research interests include acoustic beacon signal processing and detection.

SHILIANG FANG received the M.S. and Ph.D. degrees from Southeast University, Nanjing, China, in 1986 and 2009, respectively. He is currently a Professor with the Key Laboratory of Underwater Acoustic Signal Processing, Ministry of Education, Southeast University. His research interests include signal processing, target detection, parameter estimation, and underwater target classification.

SHUXIA HUANG received the B.S. degree in information engineering from Southeast University (SEU), Nanjing, China, in 2014, where she is currently pursuing the Ph.D. degree with the Key Laboratory of Underwater Acoustic Signal Processing, Ministry of Education. Her research interests include active sonar signal processing, acoustic parameter estimation, and underwater communication.